Selective Absorption of Hydrophobic Cations in Nanostructured Porous Materials from Crosslinked Hydrogen-Bonded Columnar Liquid Crystals

ARTICLE *in* ADVANCED MATERIALS INTERFACES · MAY 2015

DOI: 10.1002/admi.201500022

6 AUTHORS, INCLUDING:

Huub van Kuringen

Technische Universiteit Eindhoven

8 PUBLICATIONS **94** CITATIONS

SEE PROFILE

Ilja Voets

Technische Universiteit Eindhoven

65 PUBLICATIONS **1,121** CITATIONS

SEE PROFILE

Albertus P H J Schenning

Technische Universiteit Eindhoven

295 PUBLICATIONS **14,386** CITATIONS

SEE PROFILE

Selective Absorption of Hydrophobic Cations in Nanostructured Porous Materials from Crosslinked Hydrogen-Bonded Columnar Liquid Crystals

*Gerardus M. Bögels, Huub P. C. van Kuringen, Ivelina K. Shishmanova, Ilja K. Voets, Albertus P. H. J. Schenning, and Rint P. Sijbesma**

A nanostructured porous material is obtained by crosslinking of a self-assembled system consisting of columnar liquid crystals with polyamines and removal of the template. For this purpose, a columnar liquid crystal with liquid crystalline properties at room temperature is synthesized and fully characterized. The orthogonal self-assembly of the columnar liquid crystal with polyamines (i.e., PPI dendrimers) results in the formation of nanosegregated structures. When crosslinked by photopolymerization a nanostructured crosslinked material is obtained. Partial removal of the polyamine template leads to a nanostructured porous material, which is characterized and the absorbent properties are investigated. The polarity of the porous material is probed and the porous material is used for the selective absorption of cationic dye molecules.

1. Introduction

Liquid crystals (LCs) are materials which combine properties of the liquid and the crystalline state. These materials are capable of forming hierarchical structures on the nanoscale by self-assembly.[1–3] Due to the orientational and positional order of the molecules, LC materials are capable of exhibiting stimuli responsive properties. For instance, light responsive actuators,[4,5] thermoresponsive materials,[6] and chemical responsive materials have been reported.[7]

One of the applications of LCs is as building blocks for nanoporous materials.[8,9] The small size of the molecules and high degree of orientational and positional order of the molecules can provide nanostructured materials with feature sizes <5 nm and high pore densities. There are several examples of porous materials made from LCs, however, only a few have been reported from hydrogen-bonded LCs.[10–21] A class of LCs which is even less commonly investigated for its thermotropic LC properties is that of hydrogen-bonded discotic or columnar LCs. One example is of Ishida and co-workers, who demonstrate the template assisted self-assembly of columnar LCs via orthogonal ionic interactions.[13–15] Similarly, a template-assisted approach has previously been applied to block copolymers by Gohy and co-workers and Russell and co-workers.[22–31] The current work focuses on the application of the thermotropic LC properties of columnar benzene-1,3,5-tricarboxamide (BTA) LCs for the development of porous materials,[32] in particular toward the development of porous materials with highly selective absorbing properties.

Alkyl-substituted BTAs are molecules which are known to form hexagonal columnar LC phases over a broad temperature range.[33–39] The columnar structure is build up by a threefold hydrogen-bonding interaction resulting in a helical structure with a large macrodipole along the columnar axis.[40–44] Previously, we showed that the BTA motif can be used to orthogonally self-assemble with PPI dendrimers and form nanosegregated structures (viz., superlattices) at elevated temperatures.[37] Also, the structure of the material was controlled at the molecular level by the application of a variety of polyamines (i.e., branched, linear, or linear organometallic).[45]

With the current work, we demonstrate that orthogonal self-assembly of polymerizable, hydrogen-bonded, columnar LCs with polyamines (i.e., PPI dendrimers) followed by photopolymerization results in a nanostructured crosslinked material (**Figure 1**). Subsequently, partial removal of the polyamine template leads to a nanostructured porous material. Hence, a BTA

G. M. Bögels, Prof. R. P. Sijbesma
Laboratory of Supramolecular Polymer Chemistry
Department of Chemical Engineering and Chemistry
Eindhoven University of Technology, PO Box 513
5600, MB, Eindhoven, The Netherlands
E-mail: r.p.sijbesma@tue.nl

G. M. Bögels, Dr. I. K. Shishmanova, Dr. I. K. Voets, Prof. A. P. H. C. Schenning, Prof. R. P. Sijbesma
Institute for Complex Molecular Systems
Eindhoven University of Technology, PO Box 513
5600, MB, Eindhoven, The Netherlands

H. P. C. van Kuringen, Dr. I. K. Shishmanova, Prof. A. P. H. C. Schenning
Laboratory of Functional Organic Materials and Devices
Department of Chemical Engineering and Chemistry
Eindhoven University of Technology, PO Box 513
5600, MB, Eindhoven, The Netherlands

H. P. C. van Kuringen
Dutch Polymer Institute (DPI), PO Box 902
5600, AX, Eindhoven, The Netherlands

Dr. I. K. Voets
Laboratory of Macromolecular Organic Chemistry
Department of Chemical Engineering and Chemistry
Eindhoven University of Technology, PO Box 513
5600, MB, Eindhoven, The Netherlands

DOI: 10.1002/admi.201500022

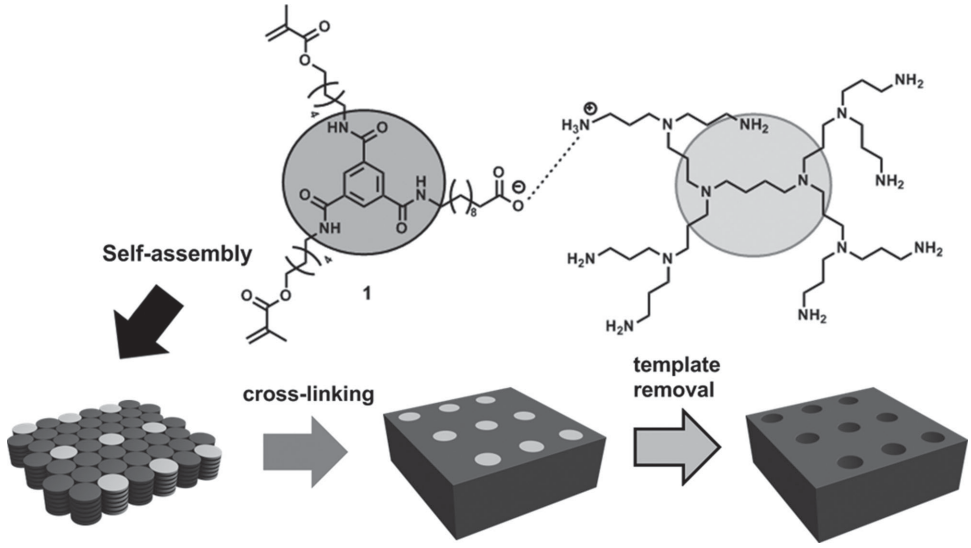

Figure 1. Concept for the formation of a nanostructured porous material from a columnar hexagonal lattice and the chemical structures of BTA **1** (dark gray) and G^2 PPI (light gray). The concept also applies to other columnar lattices.

with LC properties at room temperature (RT) was synthesized and fully characterized. Next to that, a nanostructured porous material was obtained, characterized, and the absorbent properties were investigated. The polarity of the porous material was probed and the porous material was used for the selective absorption of cationic dye molecules.

2. Design and Synthesis of the BTA

The molecular structure of BTA **1** is depicted in Figure 1. The molecular design is based on the physical properties of previously made BTAs. C_3-symmetric alkyl functionalized BTAs have a hexagonal columnar phase across a broad temperature range, e.g., C_{10}–BTA,[39] is crystalline below 50 °C, has a Col_{ho} phase up to 211 °C, and is an isotropic liquid above this temperature. Incorporation of acrylate esters results in drastic lowering of the order–disorder transition from ≈211 °C for the C_{10}–BTA to 120 °C for the acrylate BTA.[46] Furthermore, desymmetrization of alkyl BTAs from C_3-symmetric to C_2-symmetric also results in lowering of the order–disorder transitions of BTAs to 116 °C.[37] Therefore, the phase transition temperatures were expected to be even lower when both features, i.e., acrylate esters and a C_2-symmetry, are incorporated into one molecule. For chemical stability during synthesis and storage of **1**, the methacrylate ester functionality was chosen (instead of an acrylate ester) for crosslinking of the desired nanostructure. The additional methyl group makes the compound less susceptible to hydrolysis and Michael addition reactions. Furthermore, an additional carboxylic acid functionality was added to the end of one alkyl chain to form noncovalent ionic bonds with polyamines via a salt bridge. In combination with the amide hydrogen bonds between stacked BTA molecules, these orthogonal interactions promote the formation of nanosegregated structures.

The synthesis of **1** is convergent, with the alkyl tails synthesized first (**Scheme 1**) and then coupled to the BTA core. First, aminoester **5** was synthesized starting from 11-bromoundecanoic acid (**2**), S_N2 substitution of the bromide by sodium azide afforded azidoacid **3** in 95% yield, subsequent esterification gave azidoester **4** in 86% yield, and reduction of the azide afforded the free aminoester **5** in quantitative yield. So, the synthesis of aminoester **5** from 11-bromoundecanoic acid was performed in 82% overall yield over three steps. Next, the acrylate functionalized tails were synthesized starting from 6-aminohexanol (**6**). Boc-protection of **6** afforded N-Boc protected aminoalcohol **7** in quantitative yield, subsequent esterification gave acrylate ester **8** in 86% yield, and final Boc-deprotection resulted in aminoester **9** as the hydrochloride salt in quantitative yield. The synthesis of aminoester **9** was performed in 86% overall yield over three steps and was directly used as the hydrochloride salt in the next reaction without further purification.

Finally, the C_2-symmetric core structure was synthesized by partial hydrolysis of trimethyl benzene-1,3,5-tricarboxylate (**10**). By using the optimized procedure developed by Engel et al.,[47] mono carboxylic acid **11** was obtained in 97% yield. Next, Steglich esterification of carboxylic acid **11** with aminoester **5** resulted in the formation of mono amide **12** in 58% yield. Mild hydrolysis of the dimethyl ester of **12** afforded diacid **13** in 99% yield. Subsequently, the diacid **13** was converted to the diacid chloride and directly coupled with freshly prepared aminoester **9** to obtain BTA **14** in 67% yield over two steps. Final deprotection of the *tert*-butyl ester gave BTA **1** quantitatively, which resulted in an overall yield of 37% over six steps. BTA **1** was fully characterized by ^{1}H-NMR, ^{13}C-NMR, FT-IR, and mass analysis (see the Supporting Information).

3. Thermotropic Liquid Crystalline Properties of the BTA

The thermotropic LC properties of **1** were studied by polarized optical microscopy (POM), X-ray diffraction (XRD), and FT-IR (**Figure 2**).[48] The POM image with crossed polarizers shows **1** is anisotropic at room temperature and when heated to 35 °C

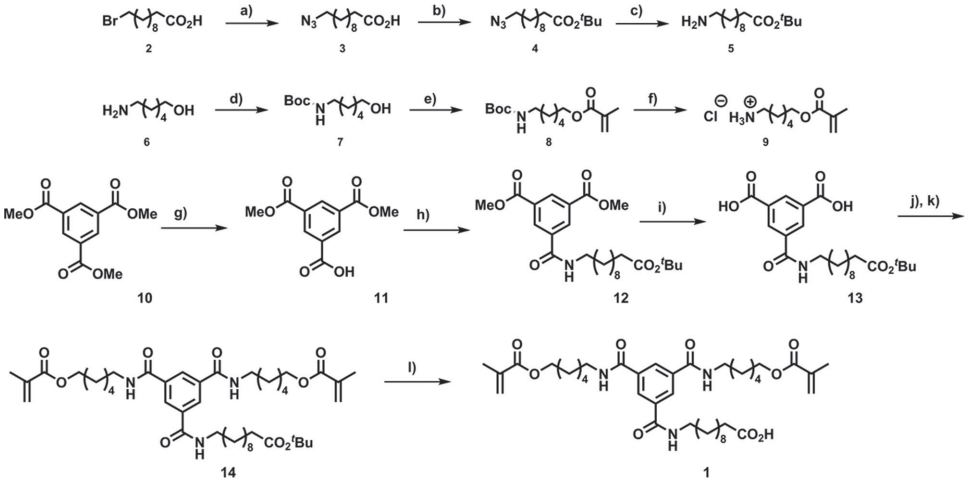

Scheme 1. A) Synthesis of aminoesters **5** and **9**, and B) the convergent synthesis of BTA **1**. a) NaN_3, DMSO, RT, 2 h (95%); b) Boc_2O, DMAP, ^tBuOH, RT, 2 h (86%); c) NH_3, MeOH, Pd/C, H_2, 70 psi, RT, 1 h (Quant.); d) Boc_2O, DCM, RT, 3 h (Quant.); e) Methacryloyl chloride, Et_3N, DCM, 0 °C, 3 h (86%); f) HCl/Et_2O, RT, 24h (Quant.); g) NaOH (aq.), MeOH, RT (97%); h) EDC.HCl, **5**, DMAP, Et_3N, DCM, –40 °C, 16 h (58%); i) LiOH, THF/H_2O, RT, 48 h, (99%); j) Ghosez's reagent, DCM, 2 h, RT; k) **9**, Et_3N, DCM, RT, 2 h (67% over two steps); l) TFA, DCM, RT, 16 h (Quant.).

it becomes an isotropic liquid (Figure S2, Supporting Information). This thermotropic property is ideal for our application to form a nanostructured porous material by orthogonal self-assembly with a polyamine, because at elevated temperatures the ionic interactions between a carboxylate and ammonium salt could form a covalent amide bond.[49] This phase behavior was also confirmed by XRD, and the highly birefringent LC phase was assigned Col_{hex}, based on the representative *q*-ratios of 1:√3:2 and a diffuse signal at 14.3 nm^{-1} of the flexible alkyl tails. Furthermore, from the XRD an intercolumnar distance of 1.94 nm was found, with an interdisc distance of 0.35 nm which is typical for LC BTA derivatives, and a density of 1.08 g cm^{-3}.

The thermotropic LC properties of BTA **1** are directly related to the hydrogen bonding properties of the molecules, as is depicted in Figure 2B. The IR-spectra show that at room temperature BTA **1** is in a hydrogen bonded state, where the OH stretch (3381 cm^{-1}) and NH stretch (3241 cm^{-1}) are sharp signals, at 1716 cm^{-1} there is both the C=O stretch of the unsaturated ester and the C=O stretch of the carboxylic acid. Furthermore, at 1641 cm^{-1} the C=O stretch of amides is present and at 1544 cm^{-1} the amide II band both confirming a hydrogen bonded state. While at 35 °C BTA **1** is not hydrogen bonded, the OH stretch (3520 cm^{-1}) and NH stretch (3321 cm^{-1}) both shift to higher wavenumbers and become much broader. Also the C=O stretch of the amides (1638 cm^{-1}) and the amide II band (1537 cm^{-1}) slightly shift to a lower wavenumber indicating a non-hydrogen bonded state.[43]

4. Orthogonal Self-Assembly

The lattice parameters of the Col_{hex} phase of **1** indicate that when part of the BTA columns is replaced by columns of a polyamine, pores of ≈2 nm in diameter may be obtained. For the formation of a superlattice structure, the ammonium/carboxylate ionic interaction should not interfere with the hydrogen-bonding interaction between the BTA molecules. Fitié et al. have shown that a BTA polyamine superlattice is obtained when a second generation (G^2) PPI dendrimer (Figure 1) is used as the polyamine.[45] Therefore, mixtures of **1** and G^2 PPI

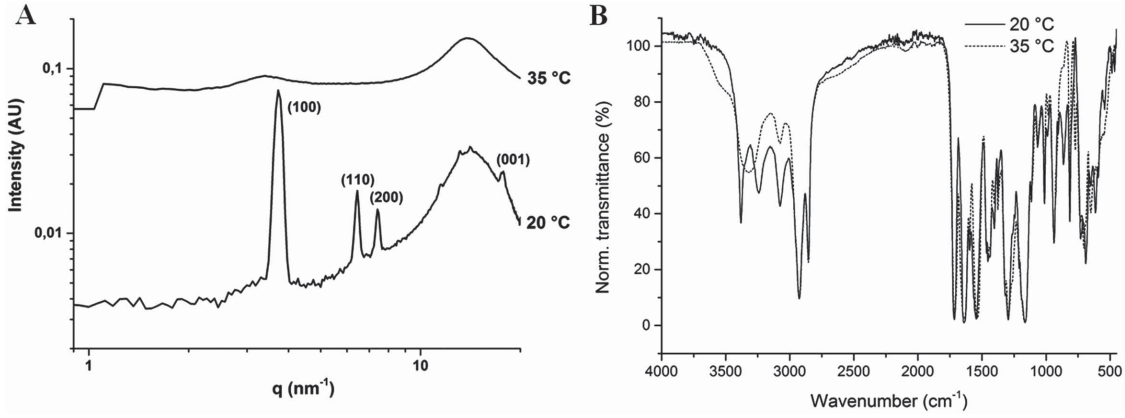

Figure 2. A) XRD plots and B) normalized FT-IR spectra of BTA **1** at 20 °C (Col_{hex}, a = 1.94 nm, c = 0.35 nm) and at 35 °C (isotropic).

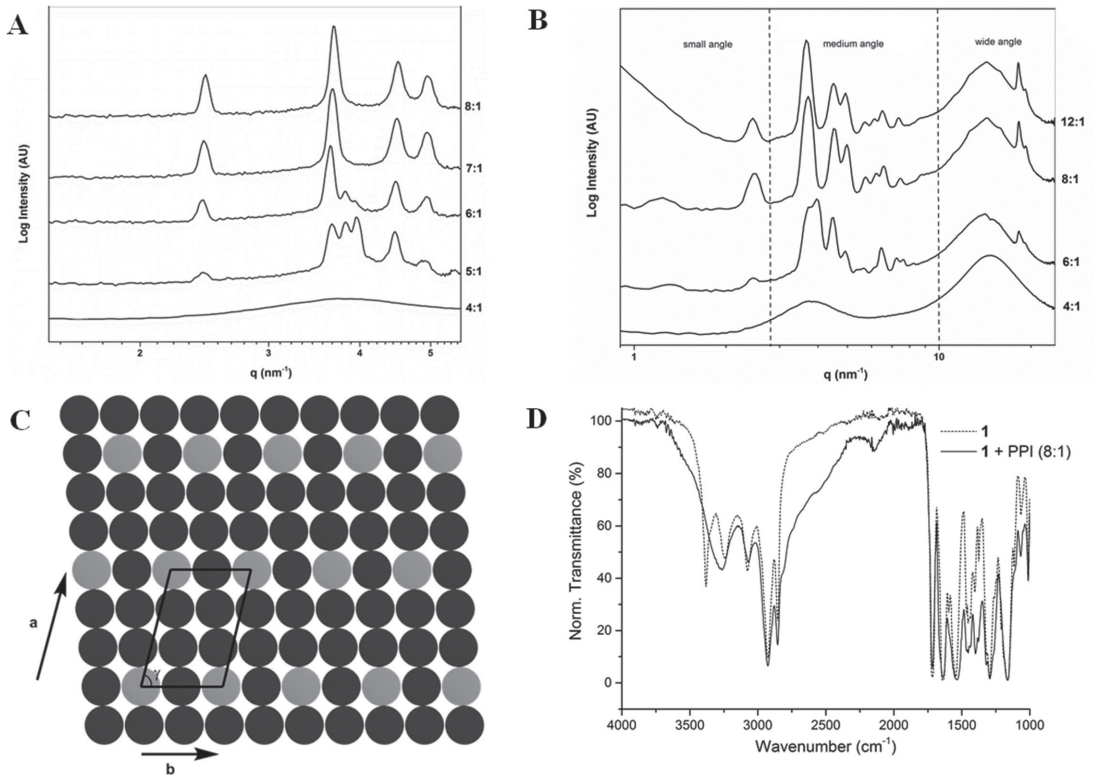

Figure 3. A) SAXS, B) WAXS of mixtures between 1 and G^2 PPI dendrimer at room temperature (molar ratios, 1:G^2 PPI). C) Structural interpretation with unit cell parameters: $a = 5.30$ nm; $b = 3.53$ nm; $c = 0.35$ nm (interdisc distance); $\gamma = 75.2°$, BTA 1 = black, PPI dendrimer = gray. D) FT-IR of 1 and 1 + G^2 PPI (8:1) at room temperature.

with molar ratios varying between 4:1 and 12:1 were prepared and the structure of the LC phases was investigated with small angle X-ray scattering (SAXS) (**Figure 3**A). At a molar ratio of 4:1 (**1** : G^2 PPI) only a very broad signal at 3.82 nm^{-1} was observed. At a 5:1 molar ratio, more and sharper signals were obtained, indicating the formation of one or more well-ordered phases. Upon increasing the molar ratio further from 5:1 up to 8:1 the signal at 3.68 nm^{-1} increased in intensity and the signals at 3.83 nm^{-1} and 3.97 nm^{-1} disappeared.

The changes in SAXS indicate that in the 5:1 mixture, two phases are present, one of which remains at an 8:1 molar ratio, where stoichiometric amounts of amine and carboxylic acid groups are present. The POM image of the 8:1 molar ratio shows birefringence between crossed polarizers (Figure S3, Supporting Information), verifying the anisotropic nature of the mixture.

Further analysis of the mixtures by wide angle X-ray scattering (WAXS) showed signals in the small angle regime, indicating that a superlattice was formed (Figure 3B). In the medium angle regime, the intercolumnar reflections were found and in the wide angle regime the broad signal corresponding to the "molten" alkyl chains and interdisc distance are present. A full interpretation of the superlattice structure can be found in Table S1, Supporting Information. The scattering data were consistent with a columnar oblique superlattice (Figure 3C) with unit cell parameters $a = 5.30$ nm, $b = 3.53$ nm, $c = 0.35$ nm, and $\gamma = 75.2°$. This gives a volume of the unit cell of 6.33 nm^3. Based on comparison with the volume of the unit cell of the Col_{hex} phase of **1** (1.14 nm^3), we propose that each unit cell of the superlattice contains five molecules of **1** and one column of dendrimer with 5/8 of a molecule fitting in a height of 0.35 nm. The volume of the unit cell of the superlattice structure resulted in a density of 1.17 g cm^{-3}, slightly higher than the weighted average density of 1.07 g cm^{-3} of the separate components.[50] This shows that the noncovalent ionic bonds between the components increases the density of the system.

The FT-IR spectrum of the 8:1 mixture (Figure 3D) shows that the NH stretch vibration at 3263 cm^{-1} of the hydrogen-bonded amide is still present in the complex, however, this band is slightly broadened due to overlap with the very broad NH stretch of the ammonium. Furthermore, the C=O stretch of the amides is at 1639 cm^{-1} and the amide II band became broader and overlaps with the carboxylate C=O stretch at 1535 cm^{-1}, while the intensity of the C=O stretch band at 1717 cm^{-1} decreases and the OH stretch band at 3382 cm^{-1} disappears because of disappearance of the free carboxylic acid. This is consistent with the presence of hydrogen-bonded amide groups in combination with ionic interactions between ammonium and carboxylate groups.

5. Orthogonal Self-Assembly with Other Polyamines

In order to investigate the versatility of the orthogonal self-assembly, several different amines were tested for the formation

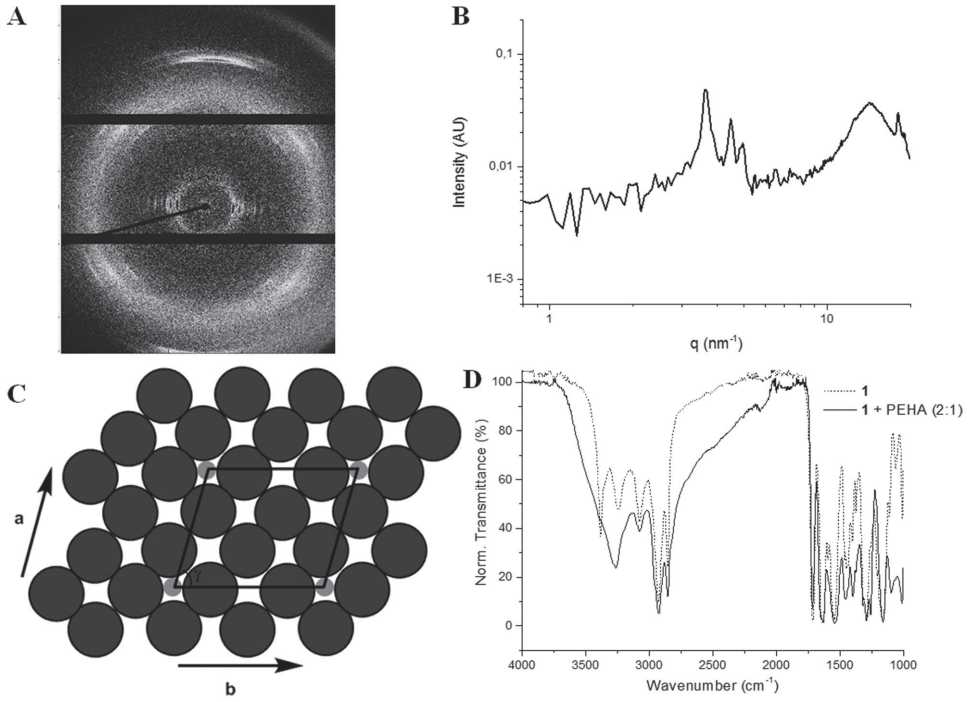

Figure 4. A) 2D-WAXS of the 2:1 mixture of BTA **1** and PEHA at room temperature, B) corresponding 1D plot, and C) proposed structural interpretation, a = 4.38 nm, b = 5.38 nm, c = 0.35 nm (interdisc distance), and γ = 73.5°, BTA = black and PEHA = gray. D) FT-IR of **1** and **1** + PEHA (2:1) at room temperature.

of LC mixtures. When combining BTA **1** with pentaethylenehexamine (PEHA) in a 2:1 molar ratio, also a LC mixture was obtained. The POM image of the mixture showed a similar type of texture as the mixture with the dendrimer (Figure S4, Supporting Information), and also in WAXS a similar structure was found (**Figure 4**).

The full interpretation of the nanosegregated structure is shown in Table S2, Supporting Information. The unit cell parameters were comparable to that of **1** with the PPI dendrimer, i.e., a = 4.38 nm; b = 5.38 nm; c = 0.348 nm, and γ = 73.5°. This was also confirmed by the density, which is 1.07 g cm^{-3} for a cell volume of 7.86 nm^3.[50] This density is slightly higher than the weighted average density of the separate components (1.04 g cm^{-3}), due to the ionic interactions between the molecules. Based on a comparison with the volume of the unit cell of the Col_{hex} phase of **1** (1.14 nm^3), we propose that each unit cell of the superlattice contains six molecules of **1** and 3 molecules of PEHA (Figure 4C). The proposed lattice has all three molecules of PEHA at one interstitial site and the organization of BTA columns within the cell is in line with the dominance of (300), (030), and (330) reflections. However, the position of the PEHA molecules inside the unit cell cannot be determined from the small number of observed reflections. There are still several ways to distribute PEHA molecules among multiple interstitial sites within the same unit cell.

Moreover, according to IR-spectroscopy the orthogonal noncovalent interactions in the 2:1 mixture are present (Figure 4D). The IR-spectrum of the 2:1 mixture is very similar to the IR-spectrum of the 8:1 mixture of **1** with PPI. The NH stretch band is located at 3261 cm^{-1}, the C=O stretch of the amides is present at 1632 cm^{-1}, and the amide II band is at 1544 cm^{-1}. Therefore, we conclude that the BTA molecules are present in the hydrogen bonded state. The NH stretch is slightly broader due to overlap with the NH stretch band of the ammonium group. Furthermore, the C=O stretch band at 1717 cm^{-1} decreased in intensity, while the band at 1544 cm^{-1} became broader, showing the conversion from a carboxylic acid to carboxylate. So, both the hydrogen bonding properties as well as the ionic interactions are present in the 2:1 mixture of BTA **1** and PEHA.

Other amines (e.g., piperazine, triazanonane, heptakis(6-aminoethylthiodeoxy)-β-cyclodextrin, diethylenetriamine, 1,12-diaminoundecane, O,O′-bis(3-aminopropyl)diethylene glycol, bis(3-aminopropyl)piperazine, DBU, DABCO, N,N,N′,N′,N″,N″-pentamethyldiethylenetriamine, hexamethylenetetramine or 2,6-di *t*-butylpyridine) did not form LC mixtures (data not shown). Either macrophase separation was observed or the mesophase was absent. It appears that a balance must be met between the hydrophobic BTA and hydrophilic amine. Apparently, this can only be achieved with a polyamine as the hydrophilic component.

6. Crosslinking of the Superlattice Structure

The nanostructured material consisting of an 8:1 molar ratio between BTA **1** and PPI dendrimer was fixated in a polymer network by UV-irradiation for 10 min under nitrogen atmosphere of mixtures containing 1.0 wt% photoinitiator (Irgacure 819). According to FT-IR analysis of the C=C bending vibration band (815 cm^{-1}), 67% of the methacrylate groups had reacted after irradiation, resulting in a crosslinked polymer

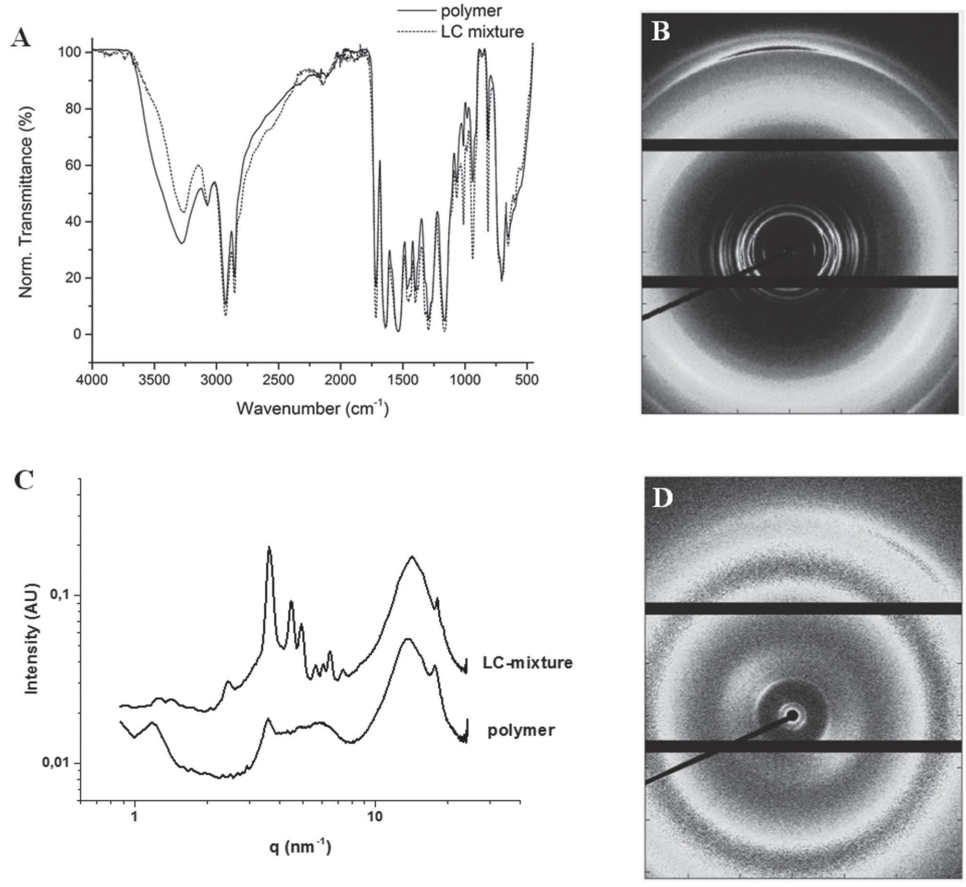

Figure 5. A) FT-IR of **1** and PPI (8:1) before and after photopolymerization, B) 2D-WAXS pattern of planar aligned **1** and PPI (8:1), C) azimuthally integrated plots of aligned **1** and PPI (8:1) before and after polymerization, and D) 2D-WAXS pattern of planar aligned **1** and PPI (8:1) after photopolymerization. All measurements are performed at room temperature.

material (**Figure 5**A). Longer irradiation did not result in higher crosslinking. Post-irradiation heating of the sample for several minutes at 100 °C resulted in >90% crosslinking. However, this temperature treatment resulted in loss of the hydrogen bonding interaction. Also, the C=O stretch band of the unsaturated ester at 1717 cm^{-1} has decreased in intensity, which confirms the conversion of the unsaturated ester into the saturated ester. Furthermore, a minor shift in the NH stretch band (3282 cm^{-1}) can be detected. This confirms that the orthogonal self-assembly is still present in the polymer material, since all the other vibration bands remain located at the same position. POM analysis showed that the texture of the sample did not change upon photopolymerization, remaining anisotropic with a similar birefringent texture (Figure S5, Supporting Information). According to DSC analysis of the nanostructured material, there are no phase transitions present after polymerization (Figure S6, Supporting Information).

Structural investigation was performed by WAXS on planar aligned samples prepared by application of a shear force (Figure 5B,D). Upon photopolymerization the desired planar alignment was retained in the polymer network. However, a decrease in intensity and broadening of the signals at the medium angle regime was observed, indicating that the superlattice structure was not fully retained (Figure 5C,D). The loss of intensity and increase of line width was particularly pronounced for the wide angle regime, but the most important signals are still present (Figure 5C). This is most probably caused by shrinkage, which takes place during the polymerization of the methacrylate groups, and is known to decrease the order in nanostructured LC materials.[51,52]

7. Removal of Dendrimer Template

The dendrimer was partly removed from the polymer network by washing with deionized water of pH 5.0. Extraction was followed by monitoring the pH of the solution after every subsequent washing step. When the deionized water is back at pH 5.0, the maximum amount of dendrimer is removed, which was after three extractions. The amount of removed PPI dendrimer was quantified in two ways, i.e., by elemental analysis (Table S3, Supporting Information) of the dried porous material and ^{1}H-NMR of the extracted PPI dendrimer with an internal standard in D_2O (Figure S7, Supporting Information). Both methods showed that between 29% and 44% of the dendrimer could be removed. The remainder of dendrimer must either be physically bound or chemically bound in the porous material. Displacement of physically bound dendrimer was

tested by exchange with other cations, e.g., methylene blue (MB). However, when a sample was treated with 1×10^{-3} M MB solution in sodium carbonate buffer at pH 10 for 24 h, mass spectrometry analysis of the solution showed that no exchange took place (Figure S8, Supporting Information). In case of chemical bonding, direct amidation from the ammonium/carboxylate complex is not likely, because the complexation and polymerization take place at room temperature. High temperatures are required for amidation to occur. Another possibility for chemical bond formation would be Michael addition of the amine to the methacrylate ester during the photopolymerization. Either the UV-irradiation generates enough heat for the Michael addition reaction to take place or it is a radical type of Michael addition reaction. When the photoinitiator is exposed to UV-light, radicals are generated which can subtract the proton from a primary amine, to form a radical nitrogen that can react with a methacrylate ester. The partial removal of the dendrimer template results in 44% removal of the 14 wt% of dendrimer, which gives rise to a porosity of 6%.

8. Polarity of the Porous Material

The polarity of the porous material was assayed by using Reichardt's dye (**Figure 6**), which is a polarity probe with negative solvatochromicity.[53] Because the dye does not dissolve in water, a co-solvent was applied which is fully miscible with water. To determine whether the co-solvent has an effect on the polarity of the porous material several different co-solvents were applied in a 1:1 volume ratio with the $NaHCO_3$ buffer solution. By changing the co-solvent ratio from 20% up to 80%, the changes in the polarity of the solution can be observed by eye, going from orange (polar) to purple (less polar) (Figure S9, Supporting Information), respectively. When the porous material was applied, the only difference which was observed is the amount of dye uptake (Figure 6A). The porous material absorbs less dye at a higher acetonitrile concentration, since the dye is better solvated. Moreover, the maximum wavelength (579 nm) of the dye in the porous material was independent of the buffer/co-solvent ratio. Also, by changing the co-solvent the polarity of the solution changes (Figure 6C), however, the dye in the porous material is independent of the polarity of the co-solvent (Figure 6D). This shows that the absorbance spectrum of the solvatochromic dye in the porous material is due to the polarity of the porous material and is not related to the polarity of the solvent. Moreover, the absorption band in the porous material is broad, suggesting that the dye molecules are in an environment with some heterogeneity in its polarity.

The normalized average polarity (E^N_T) was derived from the maximum wavelength, which was found to be 0.586 kcal mol^{-1}.[42] This value corresponds to literature values[53] of the solvatochromic dye in butanol (E^N_T = 0.586 kcal mol^{-1})

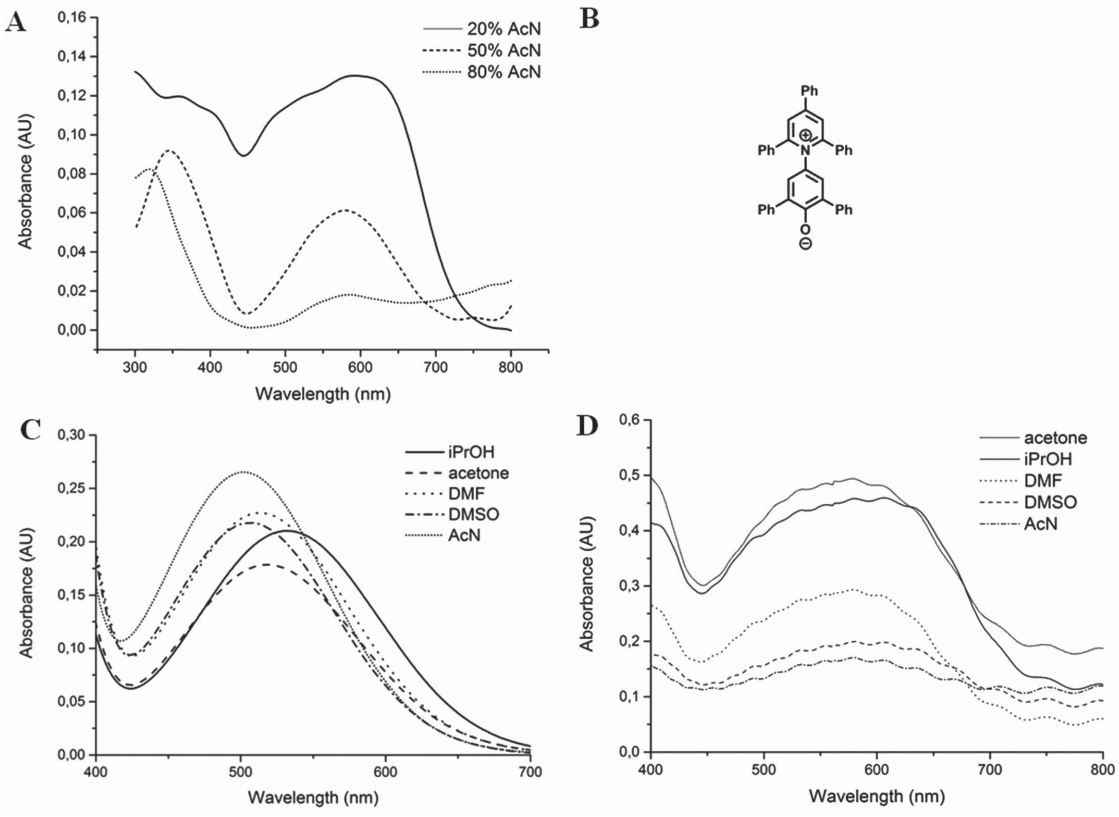

Figure 6. A) Absorbance spectra of porous material containing Reichardt's dye, with dependence of acetonitrile percentage on dye uptake and B) structure of Reichardt's dye, C) absorbance spectra of Reichardt's dye in solution, with different co-solvents applied (50% v/v), and D) absorbance spectra of porous materials containing Reichardt's dye, with different co-solvents applied (50% v/v). All experiments were performed in co-solvent mixtures with sodium bicarbonate buffer solution at pH 10. Also see Figure S8, Supporting Information.

and carboxylic acids (e.g., acetic acid E^N_T = 0.648 kcal mol^{-1} or propionic acid E^N_T = 0.611 kcal mol^{-1}). Also, by comparing the polarity of the porous material with the polarity of bilayers of dipalmitoylphosphatidylcholine (DPPC; E^N_T = 0.590 kcal mol^{-1}), this is quite similar.[54] From these comparisons, we conclude that the pores are also very hydrophobic. We speculate that this is due to the close proximity of the carboxylate anions of the BTA, which repel each other and therefore exposing more of the flexible hydrocarbon side chains toward the pores.

9. Selective Absorption of Dye Molecules

When the carboxylic acid functionalized, porous material is brought into a buffered solution of pH 10, the carboxylate anion can interact with cationic molecules. The specificity of the interaction was tested by comparing the absorption of the dye by a nonporous polymer film of pure **1** (control absorption) with a porous **1** and PPI material (total amount absorbed). For different dyes, the selectivity was tested, i.e., cationic, anionic, and neutral dyes (**Figure 7**A) by measuring the UV–vis absorbance spectra and calculating the amount of absorbed dye per weight of material according to a calibration line. This was then expressed in percentage of the total amount of carboxylates in the material which are occupied by forming a 1:1 complex with a dye molecule. The absorption behavior of the cationic dyes was compared with the anionic dyes. Furthermore, cationic dyes were more readily absorbed, while the anionic dyes were not absorbed at all. The control absorption was in most cases ≤ 1% of the total amount of absorbed dye, corresponding to adsorption of the dye to the carboxylates at the surface. In the case of MB, 78% of the total amount of carboxylates in the material formed a complex with MB, owing to the porous nature of the material.

For the neutral dye, nile red (NR), only nonspecific absorption was detected from the control, which shows the selective absorbance properties of the material. Also, NR is a solvatochromic dye which is used to probe hydrophobic pockets and has a similar size as MB. This shows that indeed the specific interaction with the carboxylates is the dominant factor, and not the hydrophobic interaction. When mixing a cationic dye (MB) with the anionic dye sodium fluorescein (SF), only the cationic dye is selectively absorbed as is shown by UV–vis spectrometry (Figure 7B). The kinetic plot shows a decrease of the MB absorbance in solution, while the SF remains constant. This can also be demonstrated visually (Figure S10, Supporting Information). The mixed solution has a green color, while after addition of the porous material, the material becomes blue in a yellow solution, showing that also in the presence of other dyes the material selectively absorbs cationic molecules. The kinetics of the process might be very dependent on the size and shape of the pores in the material, and the alignment of the pores. This was not further investigated.

However, when a multivalent cationic dye is used (i.e., Me-G2-PPI), this only shows as much absorption as in the control measurement. Comparing the size of the three cationic dyes shows that this latter effect is due to size selectivity. The diameter of MB is 8.0 Å and is readily absorbed, CV is almost twice as large with a diameter of 15.1 Å and only modestly absorbed. Furthermore, the Me-G2-PPI dendrimer has a diameter of 43.5 Å and is not absorbed. This shows that the pore size is maximally 4.4 nm and can be around the expected size of 2.0 nm of a BTA column.

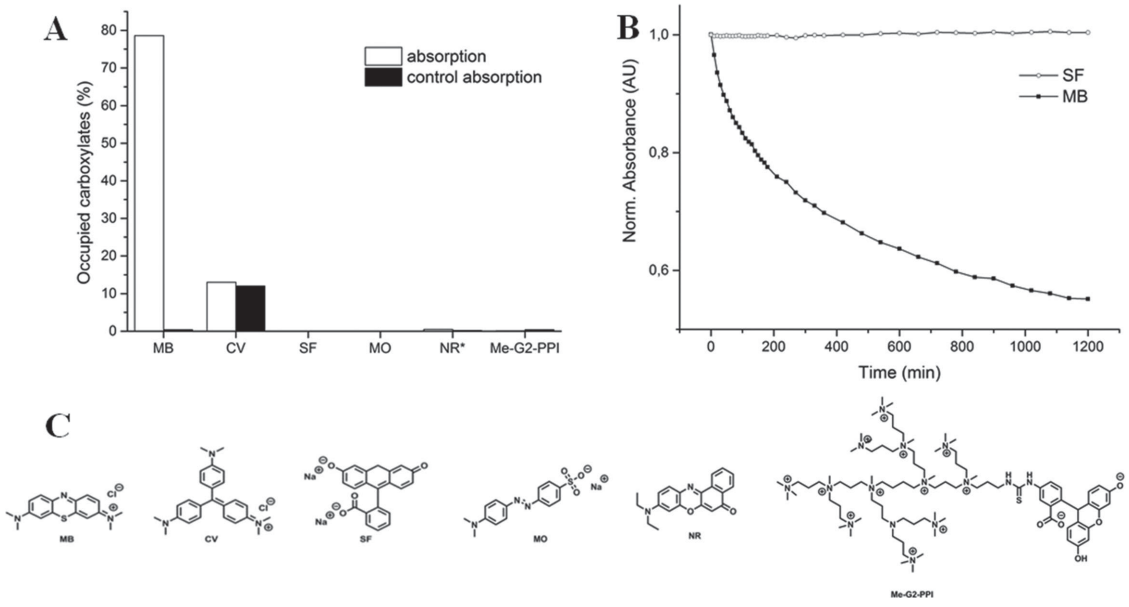

Figure 7. A) Absorption and control absorption of dyes by porous BTA material in sodium bicarbonate buffer at pH 10 after 6 h, B) normalized kinetic plot of methylene blue and sodium fluorescein absorption in solution, and C) chemical structures of the different dyes applied. MB = methylene blue, CV = crystal violet, SF = sodium fluorescein, MO = methyl orange, NR = nile red, and Me-G2-PPI = fluorescein labeled, methylated, poly(propylene imine) dendrimer of generation 2. *Mixture of AcN/$NaHCO_3$ buffer pH 10 (1:1).

10. Conclusion

The results show that orthogonal self-assembly of a polymerizable hydrogen-bonded LC phase from benzene-1,3,5-tricarboxamides combined with several polyamine template molecules results in a nanostructured porous material after photocrosslinking and partial removal of the water soluble template by extraction. A fraction of the template molecules is not removed, presumably because they are covalently bound to the network. The porous material selectively absorbs hydrophobic cationic dyes. Comparison with films polymerized in the absence of template conclusively demonstrates that templated structure formation is essential for binding of the dyes. Characterization of the polarity of the pores with Reichardt's dye shows that the pores provide an environment (E^{N}_{T} = 0.586 kcal mol^{-1}) which is similar to that of solvents such as butanol. The rather low polarity of the pores explains selectivity for binding of hydrophobic dyes. Furthermore, size selectivity for dyes with a diameter of less than ≈4 nm is observed.

Supporting Information

Supporting Information is available from the Wiley Online Library or from the author.

Acknowledgements

We gratefully thank the animation studio of the Institute of Complex Molecular Systems for the provided images. G.M.B. acknowledges Henk Janssen of SyMo Chem. B.V. for providing the PPI dendrimer and Prof. D. J. Broer for the helpful discussions. A part of the X-ray experiments was performed at the European Synchrotron Radiation Facility (ESRF, Grenoble) at the DUBBLE beamline, BM26. We are grateful for the beam time and kindly acknowledge Giuseppe Portale for the technical support. I.K.V. is grateful for financial support from The Netherlands Organization for Scientific research (NWO-ECHO-STIP Grant No. 717.013.005). This work is supported by NanoNextNL, a micro and nanotechnology consortium of the Government of the Netherlands and 130 partners and by the Ministry of Education, Culture and Science (Gravity program 024.001.035).

Received: January 14, 2015
Revised: February 12, 2015
Published online: March 23, 2015

[1] D. Demus, J. Goodby, G. W. Gray, H.-W. Spiess, V. Vill, *Handbook of Liquid Crystals*,Vol. *1*, Wiley-VCH, Weinheim, Germany **1998**.
[2] D. Demus, J. Goodby, G. W. Gray, H.-W. Spiess, V. Vill, *Handbook of Liquid Crystals*,Vol. *2B*, Wiley-VCH, Weinheim, Germany **1998**.
[3] T. Aida, E. W. Meijer, S. I. Stupp, *Science* **2012**, *335*, 813.
[4] C. L. van Oosten, C. W. M. Bastiaansen, D. J. Broer, *Nat. Mater.* **2009**, *8*, 677.
[5] S. Iamsaard, S. J. Aßhoff, B. Matt, T. Kudernac, J. J. L. M. Cornelissen, S. P. Fletcher, N. Katsonis, *Nat. Chem.* **2014**, *6*, 229.
[6] G. Wu, Y. Jiang, D. Xu, H. Tang, X. Liang, G. Li, *Langmuir* **2011**, *27*, 1505.
[7] L. T. de Haan, J. M. N. Verjans, D. J. Broer, C. W. M. Bastiaansen, A. P. H. J. Schenning, *J. Am. Chem. Soc.* **2014**, *136*, 10585.
[8] T. Kato, T. Yasuda, Y. Kamikawa, M. Yoshio, *Chem. Commun.* **2009**, *7*, 729.
[9] B. R. Wiesenauer, D. L. Gin, *Polym. J.* **2012**, *44*, 461.
[10] D. J. Broer, C. M. W. Bastiaansen, M. G. Debije, A. P. H. J. Schenning, *Angew. Chem. Int. Ed.* **2012**, *51*, 7102.
[11] A. P. H. J. Schenning, Y. C. Gonzalez-Lemus, I. K. Shishmanova, D. J. Broer, *Liq. Cryst.* **2011**, *38*, 1627.
[12] H.-K. Lee, H. Lee, Y. H. Ko, Y. J. Chang, N.-K. Oh, W.-C. Zin, K. Kim, *Angew. Chem.* **2001**, *113*, 2741.
[13] Y. Ishida, S. Amano, K. Saigo, *Chem. Commun.* **2003**, *18*, 2338.
[14] Y. Ishida, S. Amano, N. Iwahashi, K. Saigo, *J. Am. Chem. Soc.* **2006**, *128*, 13068.
[15] S. Amano, Y. Ishida, K. Saigo, *Chem. Eur. J.* **2007**, *13*, 5186.
[16] Y. Ishida, H. Sakata, A. S. Achalkumar, K. Yamada, Y. Matsuoka, N. Iwahashi, S. Amano, K. Saigo, *Chem. Eur. J.* **2011**, *17*, 14752.
[17] Y. Ishida, *Materials* **2011**, *4*, 183.
[18] K. Kishikawa, A. Hirai, S. Kohmoto, *Chem. Mater.* **2008**, *20*, 1931.
[19] C. L. Gonzalez, C. W. M. Bastiaansen, J. Lub, J. Loos, K. Lu, H. J. Wondergem, D. J. Broer, *Adv. Mater.* **2008**, *20*, 1246.
[20] J. H. Lee, *Liq. Cryst.* **2014**, *41*, 738.
[21] H. P. C. van Kuringen, G. M. Eikelboom, I. K. Shishmanova, D. J. Broer, A. P. H. J. Schenning, *Adv. Funct. Mater.* **2014**, *32*, 5045.
[22] C. G. Gamys, J.-M. Schumers, C. Mugemana, C.-A. Fustin, J.-F. Gohy, *Macromol. Rapid Commun.* **2013**, *34*, 962.
[23] C. G. Gamys, A. Vlad, O. Bertrand, J.-F. Gohy, *Macromol. Chem. Phys.* **2012**, *213*, 2075.
[24] C. G. Gamys, J.-M. Schumers, A. Vlad, C.-A. Fustin, J.-F. Gohy, *Soft Matter* **2012**, *8*, 4486.
[25] J.-M. Schumers, A. Vlad, I. Huynen, J.-F. Gohy, C.-A. Fustin, *Macromol. Rapid Commun.* **2012**, *33*, 199.
[26] H. Yu, F. Stoffelbach, C. Detrembleur, C.-A. Fustin, J.-F. Gohy, *Eur. Polym. J.* **2012**, *48*, 940.
[27] H. Ahn, S. Park, S.-W. Kim, P. J. Yoo, D. Y. Ryu, T. P. Russell, *ACS Nano* **2014**, *8*, 11745.
[28] H. Zhao, W. Gu, M. W. Thielke, E. Sterner, T. Tsai, T. P. Russell, E. B. Coughlin, P. Theato, *Macromolecules* **2013**, *46*, 5195.
[29] W. Chen, S. Park, J.-Y. Wang, T. P. Russell, *Macromolecules* **2009**, *42*, 7213.
[30] J.-T. Chen, M. Zhang, T. P. Russell, *Nano Lett.* **2007**, *7*, 183.
[31] Y. Lin, A. Böker, J. He, K. Sill, H. Xiang, C. Abetz, X. Li, J. Wang, T. Emrick, S. Long, Q. Wang, A. Balazs, T. P. Russell, *Nature (London)* **2005**, *434*, 55.
[32] S. Cantekin, T. F. A. de Greef, A. R. A. Palmans, *Chem. Soc. Rev.* **2012**, *41*, 6125.
[33] L. Brunsveld, A. P. H. J. Schenning, M. a. C. Broeren, H. M. Janssen, J. a. J. M. Vekemans, E. W. Meijer, *Chem. Lett.* **2000**, *29*, 292.
[34] L. Brunsveld, B. J. B. Folmer, E. W. Meijer, R. P. Sijbesma, *Chem. Rev.* **2001**, *101*, 4071.
[35] M. Masuda, P. Jonkheijm, R. P. Sijbesma, E. W. Meijer, *J. Am. Chem. Soc.* **2003**, *125*, 15935.
[36] A. J. Wilson, J. van Gestel, R. P. Sijbesma, E. W. Meijer, *Chem. Commun.* **2006**, *42*, 4404.
[37] C. F. C. Fitié, I. Tomatsu, D. Byelov, W. H. de Jeu, R. P. Sijbesma, *Chem. Mater.* **2008**, *20*, 2394.
[38] C. F. C. Fitié, W. S. C. Roelofs, P. C. M. M. Magusin, M. Wübbenhorst, M. Kemerink, R. P. Sijbesma, *J. Phys. Chem. B* **2012**, *116*, 3928.
[39] A. Timme, R. Kress, R. Q. Albuquerque, H.-W. Schmidt, *Chem. Eur. J.* **2012**, *18*, 8329.
[40] M. P. Lightfoot, F. S. Mair, R. G. Pritchard, J. E. Warren, *Chem. Commun.* **1999**, *19*, 1945.
[41] A. Sakamoto, D. Ogata, T. Shikata, O. Urakawa, K. Hanabusa, *Polymer* **2006**, *47*, 956.
[42] I. A. W. Filot, A. R. A. Palmans, P. A. J. Hilbers, R. A. van Santen, E. A. Pidko, T. F. A. de Greef, *J. Phys. Chem. B* **2010**, *114*, 13667.

[43] P. J. M. Stals, J. C. Everts, R. de Bruijn, I. A. W. Filot, M. M. J. Smulders, R. Martín-Rapún, E. A. Pidko, T. F. A. de Greef, A. R. A. Palmans, E. W. Meijer, *Chem. Eur. J.* **2010**, *16*, 810.
[44] R. Q. Albuquerque, A. Timme, R. Kress, J. Senker, H.-W. Schmidt, *Chem. Eur. J.* **2013**, *19*, 1647.
[45] C. F. C. Fitié, E. Mendes, M. A. Hempenius, R. P. Sijbesma, *Macromolecules* **2011**, *44*, 757.
[46] K. Hermans, I. Tomatsu, M. Matecki, R. P. Sijbesma, C. W. M. Bastiaansen, D. J. Broer, *Macromol. Chem. Phys.* **2008**, *209*, 2094.
[47] M. Engel, C. W. Burris, C. A. Slate, B. W. Erickson, *Tetrahedron* **1993**, *49*, 8761.
[48] For DSC of BTA **1** see Figure S1, Supporting Information.
[49] R. M. Lanigan, T. D. Sheppard, *Eur. J. Org. Chem.* **2013**, *33*, 7453.
[50] For the calculation of the densities, see the Supporting Information.
[51] M. P. Patel, M. Braden, K. W. M. Davy, *Biomaterials* **1987**, *8*, 53.
[52] N. Satsangi, H. R. Rawls, B. K. Norling, *J. Biomed. Mater. Res. B* **2005**, *74B*, 706.
[53] C. Reichardt, *Chem. Rev.* **1994**, *94*, 2319.
[54] K. A. Zachariasse, Nguyen Van Phuc, B. Kozankiewicz, *J. Phys. Chem.* **1981**, *85*, 2676.